Physical Layer Security for Multi-User MIMO Visible Light Communication Systems with Generalized Space Shift Keying

Nuğman Su, *Student Member, IEEE,* Erdal Panayirci, *Life Fellow, IEEE,* Mutlu Koca, *Senior Member, IEEE,* Anil Yesilkaya, *Student Member, IEEE,* H. Vincent Poor, *Life Fellow, IEEE,* and Harald Haas, *Fellow, IEEE*

***Abstract*—We consider the physical layer security (PLS) of multi-user (MU) multiple-input-multiple-output visible light communication (VLC) systems with an eavesdropper (Eve) and propose a novel spatial constellation design technique based on generalized space shift keying (MU-GSSK-SCD). The received signals of the legitimate users are optimized jointly, such that their bit error ratios (BERs) are minimized and Eve's BER is significantly degraded. The emission power of randomly selected light-emitting diodes is adjusted, by exploiting users' channel state information at the transmitter. Our strategy ensures that legitimate users receive confidential messages fully in an undistorted fashion, while any meaningful leakage to Eve is strongly prohibited, without any artificial noise addition. Every user can decode only its information, hence inter-user security is also guaranteed. The PLS improvements are presented in terms of both BERs and achievable secrecy rates in practical VLC scenarios. For various user configurations, it is shown that MU-GSSK-SCD increases the BER at Eve to the 0.5 level, while providing minimized BERs to the legitimate users. The achievable secrecy rate region is derived for MU-GSSK-SCD and it is shown that full secrecy can be achieved at 0 dB signal-to-noise ratio (SNR) level with a user separation as small as 90 cm.**

***Index Terms*—Physical layer security (PLS), multi-user communication, secrecy rate region, visible light communication (VLC), generalized space shift keying (GSSK), multiple-input-multiple-output channels (MIMO).**

I. Introduction

The evolution of wireless communication systems and the way people use their mobile devices are constantly inducing one another for high data rates, low latency, high reliability, and availability. To address this data-centric era of wireless connectivity demands efficiently, two important factors; (i) utilization of a higher frequency portion of the spectrum and (ii) deployment of multiple transmitter (TX) / receiver (RX) units are set to be the core components of fifth generation (5G) and beyond wireless communication networks [1]. Firstly, the frequencies above 30 GHz, referred to as the mm-Wave band, is started to be considered as a viable solution for delivering broadband wireless data access in the literature. However, due to the high path loss characteristic of the electromagnetic (EM) wave in the $30-300$ GHz band, mmWave systems would require the deployment of many access points (APs) even for a very small area, compared to conventional radio systems. Here, the optical wireless communications (OWC), in a broader extend light fidelity (LiFi), offers the utilization of both visible light (VL) and infrared (IR) bands to address the mentioned problems in an radio frequency (RF) non-interfering way. Since LiFi networks utilize the existing illumination infrastructure for seamless broadband data transmission, it offers energy and cost efficiency along with significant deployment ease. Furthermore, a significant area of spectral efficiency and secrecy could be achieved as the light cannot penetrate through opaque objects [2], [3]. Secondly, the utilization of multiple elements at both TX and RX sides, namely multiple-input-multiple-output (MIMO), have its distinct potential to increase the system capacity [4]. Also, multiple transmit and receive units could also be used to increase the system reliability and quality of service (QoS) as well as the achievable signal-to-noise ratio (SNR) and error performance. More recently, the MIMO systems are started to be used to enhance the achievable secrecy of the wireless communication systems [5], [6].

The amalgamation of both the nm-wave signalling and MIMO transmission creates the physical layer security (PLS) for the optical systems with multiple TX and/or RX units [7]–[16]. Moreover, PLS for multi-user MIMO networks for in RF and optical bands have recently drawn a significant attention from the researchers [17]–[22]. Particularly, spatial modulation (SM) is a promising MIMO transmission technique which is able to achieve enhanced error performance by deactivating some of the transmit units in an energy efficient manner [23]. Accordingly, both the signal itself (constellation symbol) and the active transmit unit index (spatial symbol) carry information in SM per transmission instant. Since only a transmit unit per symbol transmission is activated in SM, the inter-channel-interference (ICI) caused by the channel

This research has been supported in part by the Scientific and Technical Research Council of Turkey (TUBITAK) under the 1003-Priority Areas R&D Projects Support Program No. 218E034, and in part by the U.S. National Science Foundation under Grant CCF-1908308. This research was also supported in part by EPSRC under Established Career Fellowship Grant EP/R007101/1. A. Yesilkaya acknowledges the financial support from Zodiac Inflight Innovations (TriaGnoSys GmbH). H. Haas acknowledges support from the Wolfson Foundation and the Royal Society.

Nuğman Su, and Mutlu Koca are with the Wireless Communications Laboratory, Department of Electrical and Electronics Engineering, Boğaziçi University, 34342 Istanbul, Turkey (e-mail: {nugman.su; mutlu.koca}@boun.edu.tr).

Erdal Panayirci is with the Department of Electrical and Electronics Engineering, Kadir Has University, 34083 Istanbul, Turkey (e-mail: eepanay@khas.edu.tr).

H. Vincent Poor is with the Department of Electrical Engineering, Princeton University, Princeton, NJ 08544 USA (e-mail: poor@princeton.edu).

Anil Yesilkaya and Harald Haas are with the LiFi Research and Development Centre, Department of Electronics and Electrical Engineering, The University of Strathclyde, Glasgow G1 1XQ, U.K. (e-mail: {a.yesilkaya; harald.haas}@strath.ac.uk).

coupling is completely mitigated. The application of SM in the optical domain is also proposed in [24]. For further simplification in SM transmission, space shift keying (SSK) method, which omits the constellation symbols completely, is proposed in [25], [26]. However, the system simplification is obtained in exchange for the reduced spectral efficiency in SSK. Therefore, a system with high spectral efficiency and less transmission complexity, referred to as generalized space shift keying (GSSK), is proposed in [27]–[29]. In GSSK, multiple transmit units are activated per transmission instant, which essentially extends the number of transmit possibilities that could be sent by using the transmit unit indexes. Although the PLS for the SM, SSK and GSSK systems are investigated in the literature [30]–[34], there are only a few works that considered multi-user SM based systems. [35], [36].

In this paper, we extend the work in [15] to an indoor multi-user MIMO-VLC (MU-MIMO-VLC) scenario and propose the MU-GSSK-SCD technique to enhance the PLS. In this system, the AP is located on the ceiling, which is equipped with multiple transmitting light-emitting diodes (LEDs) for illumination and wireless data transfer purposes. A fixed number of the LEDs are activated for each channel use, while the rest operates for illumination only. The legitimate users and the eavesdropper are scattered within the environment and equipped with multiple photodetectors (PDs) for data reception. In order to satisfy the eye-safety requirements of the visible light communication (VLC) system, the illumination level is constrained in a preset interval by adjusting the direct-current (DC) bias level accordingly. We optimize the received signal constellations at the legitimate users jointly by adjusting the emission power of each transmitting LEDs with the channel state information (CSI) of the legitimate users. This power allocation introduces jamming for the eavesdropper only, while the legitimate users get an undistorted signal. The proposed strategy also ensures zero user-interference and does not require CSI exchange between the legitimate users. Furthermore, the achievable secrecy rate region for MU-MIMO-VLC is derived analytically. The proposed multi user-GSSK with spatial constellation design (MU-GSSK-SCD) system is simulated in a practical indoor VLC environment for various user configurations, which shows that the bit error ratio (BER) of the eavesdropper is significantly degraded. The simulation results also show that the improvement in the secrecy rate depends on the user positions relative to each other. However, the full secrecy is indeed attainable at 0 dB SNR with a user separation of 90 cm. The BER and secrecy rate results prove that the PLS of the multi user-MIMO-VLC (MU-MIMO-VLC) system is ensured with the MU-GSSK-SCD approach. The contributions of this paper can be summarized as follows:

- A novel multidimensional lattice design technique for multi-user GSSK system, namely MU-GSSK-SCD, is proposed to improve the PLS of the MU-MIMO-VLC transmission. According to our proposed approach, the emitted light intensity of the transmitting LEDs is adjusted by using the legitimate users CSI, such that the received signal constellations at the legitimate users are optimized in terms of BER.
- Multi user RF- or VLC-based MIMO communications is generally based on assigning disjoint sets of transmit antennas or LEDs to each user or cluster of users. Conversely, the multi user PLS technique proposed in this paper does not require such clustering approach. Instead, by means of a properly designed precoding at the transmitter, all available LEDs are used simultaneously for reliable and secure information transmission to each user without any multi user interference (MUI) with higher spectral efficiency.
- The proposed MU-GSSK-SCD scheme inherently generates a friendly jamming signal by the random switching of the LED, preventing any meaningful confidential information leakage to Eve. Whereas, in classical PLS-based systems, a separate jamming signal is generated for this purpose at the expense of resorting to highly directive LED arrays, suitable beamforming techniques and requiring the CSI of Eve by the transmitter as well as higher signal energy for transmission of the jamming signal.
- The achievable secrecy rate region of MU-MIMO-VLC systems by the MU-GSSK-SCD technique is derived analytically for a given number of LEDs and PDs and the secrecy performance is presented for different user separations and varying number of PDs.

The outline of this work is as follows. In Section II, we introduce the MU-MIMO-GSSK-VLC system model. Next in Section III, the MU-GSSK-SCD technique is explained in detail. The analytical secrecy rate upper bounds and the secrecy rate regions are derived in Section IV. The performance evaluations of the proposed MU-GSSK-SCD technique are presented in Section IV for various parameters and with both perfect and imperfect CSI at the legitimate users. We finalize this work with concluding remarks in Section V.

Notation: Throughout the paper, matrices and column vectors are in bold uppercase and lowercase letters, respectively. Unless stated otherwise, $\mathbf{A}_k$ and $\mathbf{a}_k$ denote the matrix $\mathbf{A}$ and the vector $\mathbf{a}$ designated to User k. The m^{th} row and n^{th} column element of the matrix $\mathbf{A}_k$ is denoted by $a_k^{m,n}$. Similarly, the m^{th} element of the vector $\mathbf{a}_k$ is given by a_k^m. The transpose, Euclidean norm, determinant and Cartesian product operations are expressed by $(\cdot)^{\mathrm{T}}$, $\|\cdot\|$, $|\cdot|$ and $\times$, respectively. The natural logarithm is denoted by $\ln(\cdot)$. The interval of numbers between a and b, including a and b, is denoted by $[a, b]$. The element-wise inequality between two vectors is given by $\preceq$. The set of all real $m \times n$ matrices are denoted by $\mathcal{R}^{m\times n}$. Statistical expectation, argument maximum, argument minimum, floor and ceiling operations are represented by $\mathrm{E}\{\cdot\}$, $\arg\max\{\cdot\}$, $\arg\min\{\cdot\}$, $\lfloor\cdot\rfloor$ and $\lceil\cdot\rceil$, respectively. Mutual information, entropy and conditional entropy are denoted by $\mathbb{I}(\cdot;\cdot)$, $\mathbb{H}(\cdot)$ and $\mathbb{H}(\cdot|\cdot)$, respectively.

II. Multi User MIMO-GSSK-VLC System Model

In this paper, we consider an indoor VLC system, where the AP (Alice) is equipped with N_t LEDs, and K legitimate users and Eve are equipped with N_r PDs each. The most straightforward approach for realizing the VLC with off-

the-shelf optical components is intensity-modulation-direct-detection (IM/DD). Accordingly, the information is encoded onto changes in instantaneous light intensity at the TX side. As the rate of change of light intensity is in the order of MHz region, this changes are not visible to the human eye. However, the subtle changes in the instantaneous light intensity can be detected by the PDs at the RX side to retrieve the information. Unlike the conventional RF systems, the small scale fading effects are lacking in IM/DD systems. The reason for this is the significantly large area of the PD devices compared to the operation wavelength (nm). Therefore, the integration of spontaneously emitted light-waves, whose phase values are uniformly distributed between $[-\pi, \pi]$, over a large area yields an average phase of zero. Furthermore, it has been reported in [37], [38] that the majority of the users experience a line-of-sight (LoS) channel as long as they are from the corners of the room. Hence, we can deduce that the multipath richness is minimal in MIMO-VLC applications, in other words, LoS component dominates the effective channel. The LoS channel coefficients are practically taken as the effective OWC channel in this work without loss of generality. We can describe the LoS coefficients between the t^{th} transmitter of Alice and the r^{th} receiver of the k^{th} user as in [39] as follows:

$$h_k^{r,t} = \frac{(\beta+1)A_{\text{PD}}}{2\pi(d_k^{r,t})^2}\cos^{\beta}(\phi_k^{r,t})\cos(\theta_k^{r,t})\mathbb{1}_{\Psi_{1/2}}(\theta_k^{r,t}). \tag{1}$$

Here, $\beta = -1/\log_2(\cos(\Phi_{1/2}))$ is the Lambertian emission order of the light source, where $\Phi_{1/2}$ is the semi-angle of the half-power of the transmitting LED. A_{PD} stands for the effective area of the non-imaging PD. The parameters $d_k^{r,t}$, $\phi_k^{r,t}$ and $\theta_k^{r,t}$ indicate the distance, the angle of emergence and the angle of incidence between the t^{th} transmitter and the r^{th} receiver of the k^{th} user, respectively. The function

$$\mathbb{1}_{\Psi_{1/2}}(\theta_k^{r,t}) = \left\{ \begin{array}{ll} 1, & \text{if } ||\theta_k^{r,t}|| \leq \Psi_{1/2} \\ 0, & \text{otherwise} \end{array} \right\} \tag{2}$$

indicates whether the incidence angle is within the field-of-view (FOV) of the PD. The parameter $\Psi_{1/2}$ is the half-angle of the FOV of the PD. The channel matrix between Alice and k^{th} user can be constructed as

$$\mathbf{H}_k = \begin{bmatrix} h_k^{1,1} & h_k^{1,2} & \dots & h_k^{1,N_t} \\ h_k^{2,1} & h_k^{2,2} & \dots & h_k^{2,N_t} \\ \vdots & \vdots & \ddots & \vdots \\ h_k^{N_r,1} & h_k^{N_r,2} & \dots & h_k^{N_r,N_t} \end{bmatrix}. \tag{3}$$

The complete architecture for the proposed multi-user MIMO-GSSK-VLC system is shown in Fig. 1. This architecture is distinguished from the conventional MU-MIMO-GSSK systems with the novel SCD and the corresponding power optimization technique, which will be discussed in the next section. We employ intensity modulated VLC, where the information is encoded on the emitted light intensity around a constant level. This is provided by driving the LEDs with a varying current around a DC bias level (B_{DC}), so that bipolar signals are encoded on the unipolar light intensity as reported in [40]. In GSSK-VLC, N_a LEDs are activated (intensity modulated) for each channel's use, while the other LEDs provide illumination only. For MU-GSSK, a joint bit sequence is broadcasted over the active LEDs to all users. For a GSSK system, the total number of bits that can be broadcasted by the AP per channel use is

$$N_B = \left\lfloor \log_2 \binom{N_t}{N_a} \right\rfloor. \tag{4}$$

Each broadcast is designed to deliver every user its designated information only, which is equal to $N_B^{(k)}$ bits per channel use (bpcu). Therefore

$$N_B = \sum_{k=1}^{K} N_B^{(k)}. \tag{5}$$

For each channel use, an information symbol is generated for the k^{th} user, from their designated symbol alphabet, $\mathcal{C}_k$, which is defined as

$$\mathcal{C}_k = \{\mathbf{b}_{k,1}, \mathbf{b}_{k,2}, \dots, \mathbf{b}_{k,i_k}, \dots, \mathbf{b}_{k,M_k}\}. \tag{6}$$

Here, $M_k = 2^{N_B^{(k)}}$ is the number of symbols in $\mathcal{C}_k$ and $i_k \in \{1, 2, \dots, M_k\}$. The variable $\mathbf{b}_{k,i_k}$ denotes the bit sequence that corresponds to the i_k^{th} information symbol of the k^{th} user and is defined as

$$\mathbf{b}_{k,i_k} = [b_{k,i_k}^{(1)}, b_{k,i_k}^{(2)}, \dots, b_{k,i_k}^{(\ell)}, \dots, b_{k,i_k}^{N_B^{(k)}}], \tag{7}$$

where ℓ is the bit index. For each channel use, a joint bit sequence is constructed by concatenating $\mathbf{b}_{k,i_k}$ for $k = 1, 2, \dots, K$ in the given order. The constructed joint bit sequence represents a joint symbol from the joint symbol alphabet,

$$\begin{aligned} \mathcal{C}_{\mathcal{S}} &= \mathcal{C}_1 \times \mathcal{C}_2 \times \cdots \times \mathcal{C}_k \times \cdots \times \mathcal{C}_K \\ &= \{\mathbf{b}_{\mathcal{S},1}, \mathbf{b}_{\mathcal{S},2} \dots, \mathbf{b}_{\mathcal{S},s}, \dots, \mathbf{b}_{\mathcal{S},M_{\mathcal{S}}}\}, \end{aligned} \tag{8}$$

where $\times$ denotes the Cartesian product operation and $M_{\mathcal{S}} = \prod_k M_k$. The element $\mathbf{b}_{\mathcal{S},s}$ is the bit sequence, representing s^{th} joint symbol, and defined as

$$\mathbf{b}_{\mathcal{S},s} = [\mathbf{b}_{1,i_1}, \mathbf{b}_{2,i_2}, \dots, \mathbf{b}_{k,i_k}, \dots, \mathbf{b}_{K,i_K}]. \tag{9}$$

Note that as mentioned above, $\mathbf{b}_{k,i_k}$ is the bit sequence for the i_k^{th} information symbol of the k^{th} user from (6). The symbol index s can be found by modified base conversion as follows.

$$s = \sum_{k=1}^{K-1} \left((i_k - 1) \prod_{j=k+1}^{K} M_j \right) + i_K. \tag{10}$$

Therefore, a joint bit sequence $\mathbf{b}_{\mathcal{S},s}$ conveys the information symbols $\{i_1, i_2, \dots, i_K\}$ of Users $k = 1, 2, \dots, K$ respectively. For each channel use, a selected $\mathbf{b}_{\mathcal{S},s}$ is broadcasted over the MU-GSSK-VLC channel by activating N_a out of N_t LEDs, whose indices are chosen randomly and stored in

$$\mathbf{I}_{\mathcal{S},s} = [I_{\mathcal{S},s}^{(1)}, I_{\mathcal{S},s}^{(2)}, \dots, I_{\mathcal{S},s}^{(\ell)}, \dots, I_{\mathcal{S},s}^{(N_a)}]^T, \tag{11}$$

where the indices of the active LEDs, $I_{\mathcal{S},s}^{(\ell)}$ and $I_{\mathcal{S},s}^{(\ell')}$, are distinct random integers from $[1, N_t]$ for $\ell \neq \ell'$ and $\ell, \ell' = 1, \dots, N_a$.

The emitted light intensity of all LEDs are determined by a constant DC bias level, B_{DC}, and the intensity variations

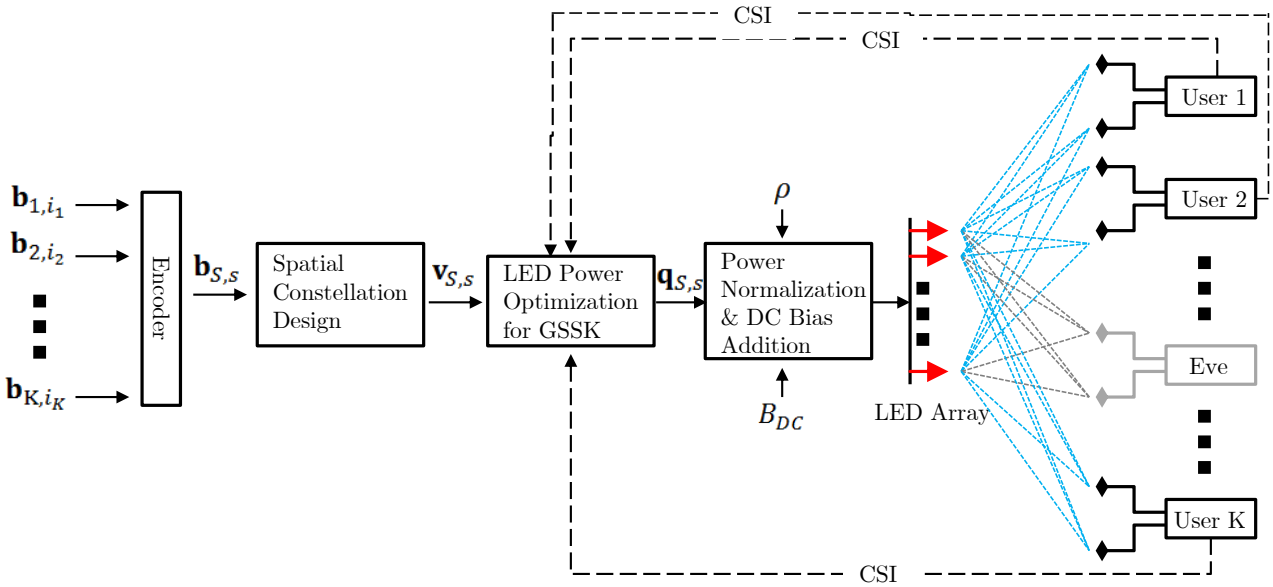

Fig. 1: System architecture for the multi-user MIMO-GSSK-VLC with SCD.

around it that carry information for $\mathbf{b}_{\mathcal{S},s}$. It is denoted by $\mathbf{q}_{\mathcal{S},s} \in \mathcal{R}^{N_t \times 1}$. Both $\mathbf{q}_{\mathcal{S},s}$ and B_{DC} are designed according to the proposed MU-GSSK-SCD scheme in the following section. Consequently, the corresponding received signals by the k^{th} user and Eve become

$$\mathbf{y}_k = \mathbf{H}_k \left(\mathbf{q}_{\mathcal{S},s} + [(B_{\text{DC}})_{\times N_t}]^T \right) + \mathbf{n}_k, \tag{12a}$$

$$\mathbf{y}_e = \mathbf{H}_e \left(\mathbf{q}_{\mathcal{S},s} + [(B_{\text{DC}})_{\times N_t}]^T \right) + \mathbf{n}_e, \tag{12b}$$

where $\left(\mathbf{q}_{\mathcal{S},s} + [(B_{\text{DC}})_{N_t \times 1}]^T \right)$ denotes the emitted light intensity of all LEDs, and $[(B_{\text{DC}})_{N_t \times 1}]^T$ is the DC bias vector. In (12), $\mathbf{H}_k$, $\mathbf{H}_e \in \mathcal{R}^{N_r \times N_t}$ are the CSI of the k^{th} legitimate user and Eve. These channel matrices are obtained from (3) and are available at the AP. The variables $\mathbf{y}_k, \mathbf{y}_e \in \mathcal{R}^{N_r \times 1}$ are the received signal vectors at the k^{th} user and Eve. The noise vectors, $\mathbf{n}_k, \mathbf{n}_e \in \mathcal{R}^{N_r \times 1}$, are zero mean Gaussian random vectors with the covariance matrices $\sigma_k^2 \mathbf{I}_{N_r}$ and $\sigma_e^2 \mathbf{I}_{N_r}$, where $\mathbf{I}_{N_r}$ is the identity matrix of size $N_r \times N_r$. In the proposed MU-GSSK-SCD, the information symbols for all users are broadcasted jointly via all LEDs with $\mathbf{q}_{\mathcal{S},s}$, unlike the LED clustering approach in such as [41]–[43], where certain LEDs are designated for a single user or group of users. Notice that, only N_a LEDs are activated per channel use by (11), therefore only those entries of $\mathbf{q}_{\mathcal{S},s}$ are non-zero. Hence the columns of $\mathbf{H}_k$, which are multiplied with the remaining zero entries of $\mathbf{q}_{\mathcal{S},s}$, do not contribute to $\mathbf{y}_k$. In this work, the legitimate users are assumed to be aware of their own channel that is the case in practical communication systems, so the DC bias can be removed from $\mathbf{y}_k$ at the receiver. Therefore, the received signals can be rewritten as follows.

$$\begin{bmatrix} \mathbf{y}_1 \\ \mathbf{y}_2 \\ \vdots \\ \mathbf{y}_K \end{bmatrix} = \rho \begin{bmatrix} \tilde{\mathbf{H}}_1 \\ \tilde{\mathbf{H}}_2 \\ \vdots \\ \tilde{\mathbf{H}}_K \end{bmatrix} \tilde{\mathbf{q}}_{\mathcal{S},s} + \begin{bmatrix} \mathbf{n}_1 \\ \mathbf{n}_2 \\ \vdots \\ \mathbf{n}_K \end{bmatrix}, \tag{13}$$

where $\tilde{\mathbf{H}}_1, \tilde{\mathbf{H}}_2, \ldots, \tilde{\mathbf{H}}_K \in \mathcal{R}^{N_r \times N_a}$ are the relevant channel state matrices of the Users $1, 2, \ldots, K$, which are constructed by N_a columns of $\mathbf{H}_k$, indicated by the entries of $\mathbf{I}_{\mathcal{S},s}$ from (11). The variable $\tilde{\mathbf{q}}_{\mathcal{S},s} \in \mathcal{R}^{N_a \times 1}$ is the intensity vector of the selected N_a LEDs before the DC bias addition. The transmit power vector is normalized with ρ, which will be detailed in the following section.

III. Spatial Constellation Design for Enhanced PLS

In conventional GSSK downlink communication, spatial constellation points are specified by a set of active transmitters. For each transmitted constellation point, the destinations receive the superposition of the channel outputs of the transmitted signals. As a result, a transmitted constellation point is detected based on a received signal constellation, whose elements mainly depend on the channel coefficients, given by (1) in our case. Hence, when conventional GSSK is employed for VLC, PLS would depend on the features of the system configuration such as location and orientation of transmitters and receivers, which determine the channel conditions. However, it is possible to design the users' received signal constellations to remove the mentioned channel dependence and minimize their BERs. In fact, the BER of an optical MIMO-GSSK system is minimized in [15] for a single user by intelligent selection of the received signal constellation points at the legitimate user. In this part, we consider a multi-user MIMO-GSSK-VLC system, and minimize the BER at all legitimate users by joint spatial constellation design of all users, namely MU-GSSK-SCD. According to MU-GSSK-SCD, for every channel use, the LED intensity vector $\tilde{\mathbf{q}}_{\mathcal{S},s}$ is designed so that the received signals from (13) become

$$\mathbf{y}_k = \rho \mathbf{v}_{k,i_k} + \mathbf{n}_k, \quad 1 \leq k \leq K, \tag{14}$$

where $\mathbf{v}_{k,i_k}$ is the received signal at user k, corresponding to the i_k^{th} information symbol and ρ is the power normalization coefficient. The received signal vector $\mathbf{v}_{k,i_k}$ belongs to

$$\mathcal{V}_k : \left\{ \mathbf{v}_{k,i_k} = [v_{k,i_k}^{(1)}, v_{k,i_k}^{(2)}, \ldots, v_{k,i_k}^{(N_r)}]^T, 1 \leq i_k \leq M_k \right\}, \tag{15}$$

which is the received spatial constellation of the User k. The selection of the elements in $\mathcal{V}_k$ is crucial because it directly affects the BER performance of the k^{th} legitimate user and also Eve. In [44], it is shown that the SCD approach minimizes the BER of a user with $N_r = 1$ in an optical spatial modulation (OSM) system by maximizing the minimal pairwise Euclidean distance of the received signal constellation points while their average norm is fixed. The work in [15] generalizes the SCD framework to the MIMO setting, and shows that bipolar signal constellation is optimal in an N_r-space. In this work, the SCD approach is applied to the multi-user setting, therefore the received spatial constellations $\mathcal{V}_k$ for all k are optimally chosen to be M-ary signal constellations in N_r-space. In order for (14) to hold, $\tilde{\mathbf{q}}_{\mathcal{S},s}$ is formed such that

$$\tilde{\mathbf{H}}_k \tilde{\mathbf{q}}_{\mathcal{S},s} = \mathbf{v}_{k,i_k}, \quad 1 \leq k \leq K. \tag{16}$$

The condition in (16) should be satisfied jointly for all users. For this purpose it is rewritten as

$$\begin{bmatrix} \tilde{\mathbf{H}}_1 \\ \tilde{\mathbf{H}}_2 \\ \vdots \\ \tilde{\mathbf{H}}_K \end{bmatrix} \tilde{\mathbf{q}}_{\mathcal{S},s} = \begin{bmatrix} \mathbf{v}_{1,i_1} \\ \mathbf{v}_{2,i_2} \\ \vdots \\ \mathbf{v}_{K,i_K} \end{bmatrix} \quad \rightarrow \quad \tilde{\mathbf{H}} \tilde{\mathbf{q}}_{\mathcal{S},s} = \mathbf{v}_{\mathcal{S},s}, \tag{17}$$

where $\tilde{\mathbf{H}}$ denotes the general channel matrix and $\mathbf{v}_{\mathcal{S},s}$ is the joint received signal vector. Note that $\mathbf{v}_{\mathcal{S},s}$ is mapped to s^{th} element in the joint symbol alphabet $\mathcal{C}_{\mathcal{S}}$ from (8), just like $\mathbf{v}_{k,i_k}$ is mapped to the i_k^{th} element in User k's symbol alphabet $\mathcal{C}_k$ from (6).

In Table I, an example for the optimal $2-$user GSSK-SCD is provided. In this setting, $N_t = 6$, $N_a = 3$, $N_r = 3$ and $K = 2$, and $N_B^{(1)} = N_B^{(2)} = 2$ bpcu is transmitted to the users, satisfying (4). Thus, both users have $M_k = 2^{N_B^{(k)}} = 4$ symbols in $\mathcal{C}_k$, given by (6). In a 3-dimensional space, 4 constellation points with unit energy have the maximal Euclidean distance from each other, when they lie on the vertices of a regular tetrahedron. Therefore, the optimal spatial constellation points are found for $k = 1, 2$ as

$$\mathbf{v}_{k,1} = [\sqrt{\frac{8}{9}}, 0, -\frac{1}{3}], \qquad \mathbf{v}_{k,2} = [-\sqrt{\frac{2}{9}}, \sqrt{\frac{2}{3}}, -\frac{1}{3}],$$
$$\mathbf{v}_{k,3} = [-\sqrt{\frac{2}{9}}, -\sqrt{\frac{2}{3}}, -\frac{1}{3}], \quad \mathbf{v}_{k,4} = [0, 0, 1],$$

for $k = 1, 2$.

The transmit power vector that achieves the optimal received signal in (17) can be obtained by a zero forcing precoder, which is found by

$$\tilde{\mathbf{q}}_{\mathcal{S},s} = \left(\tilde{\mathbf{H}}^T \tilde{\mathbf{H}} \right)^{-1} \tilde{\mathbf{H}}^T \mathbf{v}_{\mathcal{S},s}. \tag{18}$$

TABLE I: Example: Optimal SCD for $2-$User GSSK-VLC $N_t = 6$,$N_a = 3$,$N_r = 3$

i_1	i_2	s	$\mathbf{b}_{\mathcal{S},s}$ (9)	$\mathbf{I}_{\mathcal{S},s}$ (11)	$\mathbf{v}_{\mathcal{S},s}$ (15)
1	1	1	$[[0,0],[0,0]]$	$[1,2,3]$	$[\mathbf{v}_{1,1}, \mathbf{v}_{2,1}]$
1	2	2	$[[0,0],[0,1]]$	$[1,2,4]$	$[\mathbf{v}_{1,1}, \mathbf{v}_{2,2}]$
1	3	3	$[[0,0],[1,0]]$	$[1,2,5]$	$[\mathbf{v}_{1,1}, \mathbf{v}_{2,3}]$
1	4	4	$[[0,0],[1,1]]$	$[1,2,6]$	$[\mathbf{v}_{1,1}, \mathbf{v}_{2,4}]$
2	1	5	$[[0,1],[0,0]]$	$[1,3,4]$	$[\mathbf{v}_{1,2}, \mathbf{v}_{2,1}]$
2	2	6	$[[0,1],[0,1]]$	$[1,3,5]$	$[\mathbf{v}_{1,2}, \mathbf{v}_{2,2}]$
2	3	7	$[[0,1],[1,0]]$	$[1,3,6]$	$[\mathbf{v}_{1,2}, \mathbf{v}_{2,3}]$
2	4	8	$[[0,1],[1,1]]$	$[1,4,5]$	$[\mathbf{v}_{1,2}, \mathbf{v}_{2,4}]$
3	1	9	$[[1,0],[0,0]]$	$[1,4,6]$	$[\mathbf{v}_{1,3}, \mathbf{v}_{2,1}]$
3	2	10	$[[1,0],[0,1]]$	$[1,5,6]$	$[\mathbf{v}_{1,3}, \mathbf{v}_{2,2}]$
3	3	11	$[[1,0],[1,0]]$	$[2,3,4]$	$[\mathbf{v}_{1,3}, \mathbf{v}_{2,3}]$
3	4	12	$[[1,0],[1,1]]$	$[2,3,5]$	$[\mathbf{v}_{1,3}, \mathbf{v}_{2,4}]$
4	1	13	$[[1,1],[0,0]]$	$[2,3,6]$	$[\mathbf{v}_{1,4}, \mathbf{v}_{2,1}]$
4	2	14	$[[1,1],[0,1]]$	$[2,4,5]$	$[\mathbf{v}_{1,4}, \mathbf{v}_{2,2}]$
4	3	15	$[[1,1],[1,0]]$	$[2,4,6]$	$[\mathbf{v}_{1,4}, \mathbf{v}_{2,3}]$
4	4	16	$[[1,1],[1,1]]$	$[2,5,6]$	$[\mathbf{v}_{1,4}, \mathbf{v}_{2,4}]$

Substituting (18) into (13), the received signals at the legitimate users become

$$\begin{bmatrix} \mathbf{y}_1 \\ \mathbf{y}_2 \\ \vdots \\ \mathbf{y}_K \end{bmatrix} = \rho \begin{bmatrix} \mathbf{v}_{1,i_1} \\ \mathbf{v}_{2,i_2} \\ \vdots \\ \mathbf{v}_{K,i_K} \end{bmatrix} + \begin{bmatrix} \mathbf{n}_1 \\ \mathbf{n}_2 \\ \vdots \\ \mathbf{n}_K \end{bmatrix}. \tag{19}$$

The expression in (19) follows, because for any matrices $\mathbf{A} \in \mathcal{R}^{N \times N}$ and $\mathbf{B} \in \mathcal{R}^{N \times M}$ for $N \leq M$, it is true that $\mathbf{A} = \mathbf{B} \left(\mathbf{B}^T \mathbf{B} \right)^{-1} \mathbf{B}^T = \mathbf{I}_N$. This can be shown easily by multiplying $\mathbf{A}$ with $\mathbf{B}^T$ from the left side and observing that $\mathbf{B}^T \mathbf{A} \equiv \mathbf{B}^T$ if $\mathbf{A} = \mathbf{I}_N$. It is also worth noting that in OWC the channels between different LEDs and PDs may be closely related depending on the user locations. Therefore, the channel coefficients are functions of the terminal locations and orientations as given in (1). In some cases, this may result in linearly dependent rows or columns in $\tilde{\mathbf{H}}$ as reported in [45] and $\mathbf{B} = \tilde{\mathbf{H}}^T \tilde{\mathbf{H}}$ may be ill-conditioned. In that case, a small perturbation ϵ, called *regularization parameter* is inserted to make the resulting matrix full rank as shown below.

$$\tilde{\mathbf{q}}_{\mathcal{S},s} = \left(\tilde{\mathbf{H}}^T \tilde{\mathbf{H}} + \epsilon \mathbf{I}_{N_a} \right)^{-1} \tilde{\mathbf{H}}^T \mathbf{v}_{\mathcal{S},s}, \tag{20}$$

where $\mathbf{I}_{N_a} \in R^{N_a \times N_a}$ denotes the unit diagonal matrix. Notice that the transmit power vector given in (20), not only achieves the optimal received signal at each legitimate user, but it also ensures zero inter-user interference as it is evident in (19). Also notice that for $K = 1$, the general channel matrix $\tilde{\mathbf{H}}$ is reduced to $\tilde{\mathbf{H}}_1$ and $\mathbf{v}_{\mathcal{S},s}$ to $\mathbf{v}_1$ by (17). In this case, the optimal transmit power vector in (20) ensures the received signals to be (19) for $K = 1$, which is identical to the solution proposed in (13) of [15]. Therefore, the proposed MU-GSSK-SCD in this work is the generalization of the single user GSSK-SCD strategy proposed in [15].

A. Transmit Power Normalization

In this section, we design the DC bias level, B_{DC}, and the power normalization coefficient, ρ. The driving current

of the LEDs must stay below a certain threshold to prevent overheating and reduction in electro-optical efficiency, as reported in [46]. Also, LEDs are expected to support communication while maintaining a constant illumination level, [47]. Therefore, the driving current must stay in $[I_{\min}, I_{\max}]$, so that both constraints are satisfied. Hence, the elements in the transmit power vector, $\tilde{\mathbf{q}}_{\mathcal{S},s}$, are forced to stay in the following current range.

$$I_{\min} < \tilde{q}_{\mathcal{S},s}^{(\ell)} < I_{\max}, \quad \ell = 1, \ldots, N_a. \tag{21}$$

For the jointly optimal $\mathcal{V}_k$'s for $k = 1, 2, \cdots, K$, it follows from (20) that $E\{\tilde{\mathbf{q}}_{\mathcal{S},s}\} = 0$. Hence, we set $B_{\text{DC}} = (I_{\min} + I_{\max})/2$. It is worth to note that, off-the-shelf white LEDs usually work below $I_{\max} = 100$ mA in average, [46]. If, for example, the preferred illumination level in the communication environment requires $B_{\text{DC}} = 75$ mA, then $I_{\min}$ is set to 50 mA. The power normalization coefficient is calculated by $\rho = (I_{\max} - I_{\min})/\max\{||\tilde{\mathbf{q}}_{\mathcal{S},s}||\}$, where $\max\{||\tilde{\mathbf{q}}_{\mathcal{S},s}||\}$ is the maximum value, the norm of the transmit power vector can take for any symbol i_k. An upper bound for this term is found by

$$\begin{aligned}\max\{||\tilde{\mathbf{q}}_{\mathcal{S},s}||\} &= \max\left\{\left|\left|\left(\tilde{\mathbf{H}}^T\tilde{\mathbf{H}}\right)^{-1}\tilde{\mathbf{H}}^T\mathbf{v}_{\mathcal{S},s}\right|\right|\right\} \\ &\prec \max\left\{\left|\left|\left(\tilde{\mathbf{H}}^T\tilde{\mathbf{H}}\right)^{-1}\tilde{\mathbf{H}}^T\right|\right|\right\}\max\{||\mathbf{v}_{\mathcal{S},s}||\}.\end{aligned} \tag{22}$$

Consequently, the received signal at the k^{th} legitimate user can be completely expressed as

$$\mathbf{y}_k = \mathbf{s}_k + \mathbf{n}_k, \tag{23}$$

where $\mathbf{s}_k$ is the observed transmitted signal by the k^{th} user and given by

$$\mathbf{s}_k = \rho\tilde{\mathbf{H}}_k\left(\tilde{\mathbf{H}}^T\tilde{\mathbf{H}} + \epsilon\mathbf{I}_{N_a}\right)^{-1}\tilde{\mathbf{H}}^T\mathbf{v}_{\mathcal{S},s} + B_{\text{DC}}\tilde{\mathbf{H}}_k, \tag{24a}$$

$$= \rho\mathbf{v}_{k,i_k} + B_{\text{DC}}\tilde{\mathbf{H}}_k, \tag{24b}$$

from which the DC bias part can be extracted with receiver's knowledge of its own channel. The transmitted signal is received by the eavesdropper as

$$\mathbf{y}_e = \rho\mathbf{H}_e\mathbf{q}_{\mathcal{S},s} + \mathbf{n}_e \tag{25}$$

$$= \rho\mathbf{H}_e\left(\tilde{\mathbf{H}}^T\tilde{\mathbf{H}} + \epsilon\mathbf{I}_{N_a}\right)^{-1}\tilde{\mathbf{H}}^T\mathbf{v}_{\mathcal{S},s} + \mathbf{n}_e. \tag{26}$$

Hence, $\mathbf{v}_{k,i_k}$ cannot be perfectly recovered at Eve for any k. The received signal $\mathbf{y}_e$ can also be expressed as

$$\mathbf{y}_e = \mathbf{s}_k + \mathbf{J}_k + \mathbf{n}_e, \tag{27}$$

where $\mathbf{J}_k$ is the jamming signal at Eve, wiretapping User k. The jamming signal $\mathbf{J}_k$ is found by

$$\mathbf{J}_k = \rho\left(\mathbf{H}_e - \mathbf{H}_k\right)\mathbf{q}_{\mathcal{S},s}. \tag{28}$$

At the legitimate users and the eavesdropper, the GSSK signal is decoded by maximum likelihood (ML) detection.

$$\hat{\mathbf{v}}_k = \arg\min_{\mathbf{v}_{k,i_k}}\left\{||\mathbf{y}_k - \rho\mathbf{v}_{k,i_k}||\right\}, \tag{29a}$$

$$\hat{\mathbf{v}}_{e,k} = \arg\min_{\mathbf{v}_{k,i_k}}\left\{||\mathbf{y}_e - \rho\mathbf{v}_{k,i_k}||\right\}, \tag{29b}$$

where $\hat{\mathbf{v}}_k$ and $\hat{\mathbf{v}}_{e,k}$ are the detected symbols at User k and the eavesdropper that wiretaps User k.

IV. Secrecy Rate Region of MU-GSSK-VLC System

The secrecy capacity of the k^{th} user for the proposed system in (23) and (27) is given in [48] and defined by

$$\begin{aligned}\mathbb{C}_{\text{GSSK}}^{(k)} &= \mathbb{I}(\mathbf{s}_k;\mathbf{y}_k) - \mathbb{I}(\mathbf{s}_k;\mathbf{y}_e), \\ &= \mathbb{H}(\mathbf{y}_k) - \mathbb{H}(\mathbf{y}_k|\mathbf{s}_k) - \left(\mathbb{H}(\mathbf{y}_e) - \mathbb{H}(\mathbf{y}_e|\mathbf{s}_k)\right),\end{aligned} \tag{30}$$

where $\mathbb{H}(\cdot)$ and $\mathbb{H}(\cdot|\cdot)$ stand for the entropy and conditional entropy, respectively. The mutual information is represented by $\mathbb{I}(\cdot;\cdot)$. Following (23), $\mathbb{H}(\mathbf{y}_k|\mathbf{s}_k)$ is found to be Gaussian entropy with

$$\mathbb{H}(\mathbf{y}_k|\mathbf{s}_k) = \frac{N_r}{2}\log_2(2\pi e\sigma_k^2). \tag{31}$$

The jamming vector in (28) can be approximated as a zero mean Gaussian random vector with the covariance matrix $\mathbb{C}_{\mathbf{J}_k}$. Then, the total noise in Eve's received signal, (27) becomes another zero mean Gaussian random vector, $\mathbf{w}_k = \mathbf{J}_k + \mathbf{n}_e$, with the covariance matrix

$$\mathbb{C}_{\mathbf{w}_k} = \mathbb{C}_{\mathbf{J}_k} + \sigma_e^2\mathbf{I}_{N_r}. \tag{32}$$

Therefore,

$$\mathbb{H}(\mathbf{y}_e|\mathbf{s}_k) = \frac{1}{2}\log_2(2\pi e|\mathbb{C}_{\mathbf{w}_k}|). \tag{33}$$

Then the secrecy capacity in (30) becomes

$$\mathbb{C}_{\text{GSSK}}^{(k)} = \frac{N_r}{2}\log_2\left(\frac{|\mathbb{C}_{\mathbf{w}_k}|^{1/N_r}}{\sigma_k^2}\right) - \left(\mathbb{H}(\mathbf{y}_e) - \mathbb{H}(\mathbf{y}_k)\right). \tag{34}$$

Since the received signal $\mathbf{y}_k$ is a mixture of M Gaussian random vectors, its entropy can be upper bounded by

$$\begin{aligned}\mathbb{H}(\mathbf{y}_k) &\le \log_2(M) + \frac{N_r}{2}\log_2\left(2\pi e\sigma_k^2\right) \\ &= \frac{N_r}{2}\log_2\left(2\pi e\sigma_k^2 M^{2/N_r}\right).\end{aligned} \tag{35}$$

A lower bound for $\mathbb{H}(\mathbf{y}_e)$ can be found by applying the entropy power inequality (EPI) to $\mathbf{y}_e = \mathbf{y}_k + \hat{\mathbf{n}}_k$, where $\hat{\mathbf{n}}_k = \mathbf{w}_k - \mathbf{n}_k$ is the significant noise term in Eve's received signal. Then by EPI, [49], we have

$$\begin{aligned}\mathbb{H}(\mathbf{y}_e) &= \mathbb{H}(\mathbf{y}_k + \hat{\mathbf{n}}_k) \\ &\ge \frac{N_r}{2}\log_2\left(2^{(2/N_r)}\mathbb{H}(\hat{\mathbf{n}}_k) + 2^{(2/N_r)}\mathbb{H}(\mathbf{y}_k)\right) \\ &= \frac{N_r}{2}\log_2\left(2\pi e|\mathbb{C}_{\hat{\mathbf{n}}_k}|^{(1/N_r)} + 2^{(2/N_r)}\mathbb{H}(\mathbf{y}_k)\right),\end{aligned} \tag{36}$$

where $\mathbb{C}_{\hat{\mathbf{n}}_k} = \mathbb{C}_{\mathbf{w}_k} - \sigma_k^2\mathbf{I}_{N_r}$ is the covariance matrix of $\hat{\mathbf{n}}_k$. Now, applying (35) and (36) to (34), we get

$$\mathbb{C}_{\text{GSSK}}^{(k)} \le \frac{N_r}{2}\log_2\left(\frac{|\mathbb{C}_{\mathbf{w}_k}|^{(1/N_r)}M^{(2/N_r)}}{\sigma_k^2 M^{(2/N_r)} + |\mathbb{C}_{\mathbf{n}_k}|^{(1/N_r)}}\right). \tag{37}$$

The achievable secrecy rate region is defined by all User secrecy rates, $\left(R^{(1)}, R^{(2)}, \ldots, R^{(K)}\right)$, which satisfy the following joint upper bound, [50].

$$\sum_{k=1}^{K} 2^{R^{(k)}} \le \sum_{k=1}^{K} 2^{\mathbb{C}_{\text{GSSK}}^{(k)}}, \tag{38}$$

where $\mathbb{C}_{\text{GSSK}}^{(k)}$ obeys (37) for $k = 1, 2, \ldots, K$. In the following, the BER and PLS performances of MU-GSSK-SCD is presented under various user configurations.

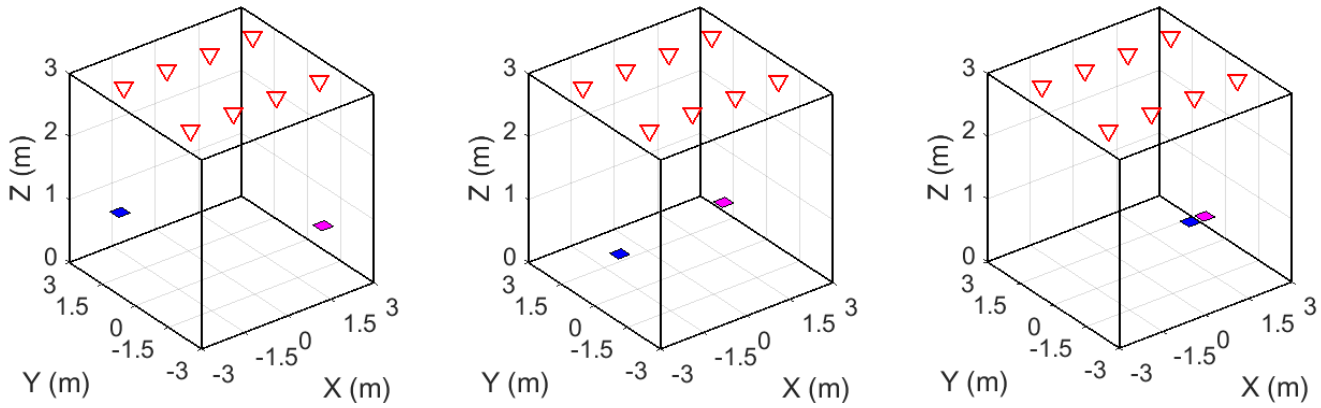

(a) (b) (c)

Fig. 2: Evaluated MIMO-VLC user configurations. User 1 and 2 are represented with blue and magenta squares, respectively. a) Scenario 1, b) Scenario 2, c) Scenario 3.

V. Simulation Results

In this section, we present the communication performances of the legitimate users and the eavesdropper under different VLC scenarios. We assume that the communication takes place in a 6 m $\times$6 m $\times$3 m indoor environment, where $N_t = 8$ LEDs are located on the ceiling. The LEDs are located at

$$\text{LED}_{\text{loc}}(x, y) = \begin{bmatrix} -2.25, & -0.75, & 0.75, & 2.25, & -2.25, & -0.75, & 0.75, & 2.25 \\ 1.5, & 1.5, & 1.5, & 1.5, & -1.5, & -1.5, & -1.5, & -1.5 \end{bmatrix}^T \text{m}. \tag{39}$$

The location vectors of the LEDs and the users are given in meters and their units will be dropped from this point on. The locations of the legitimate users and the eavesdropper differ for each scenario and are indicated in the rest of this section. The LoS channel coefficients are obtained by (1) with the following parameters.

$$\Phi_{1/2} = 60^\circ, \quad \Psi_{1/2} = 70^\circ, \quad A_{\text{PD}} = 1 \text{ cm}^2. \tag{40}$$

The other channel parameters, $\beta, d_k^{r,t}, \phi_k^{r,t}, \theta_k^{r,t}$, are obtained from the locations of the LEDs, users and the eavesdropper. Also, the emission power is assumed to be 1 W per LED.

For simulation purposes, we activate $N_a = 4$ LEDs per channel use. The reception at $K = 2$ legitimate users and the eavesdropper is performed by $N_r = 2$ PDs. The total number of bits sent per channel use is $N_B = 6$ by (4). N_B is divided evenly among the legitimate users, hence $M = 2^{N_B/2} = 8$ for both users. Thus, $\mathcal{C}_1$ and $\mathcal{C}_2$ have the cardinality of $M = 8$ and consist of the bit vectors of length $N_B/2 = 3$. The joint symbol alphabet is the Cartesian product of $\mathcal{C}_1$ and $\mathcal{C}_2$, therefore $\mathcal{C}_\mathcal{S}$ consists of $M^2 = 64$ bit vectors of length $N_B = 6$. Since $N_r = 2$ and $M = 8$, $\mathcal{V}_1$ and $\mathcal{V}_2$ are chosen to be 8$-$QAM symbol constellations. For each channel use, random bit vectors $\mathbf{b}_{1,i_1}$ and $\mathbf{b}_{2,i_2}$ are chosen from $\mathcal{C}_1$ and $\mathcal{C}_2$ respectively and their corresponding joint bit vector $\mathbf{b}_{\mathcal{S},s}$ is found from $\mathcal{C}_\mathcal{S}$. Then, $\tilde{\mathbf{q}}_{\mathcal{S},s}$ is calculated according to (20) for a signal amplitude ρ and the received signal $\mathbf{v}_{\mathcal{S},s}$, which is mapped to $\mathbf{b}_{\mathcal{S},s}$. Finally, the GSSK signal is received by all users according to (12).

A. BER Performance of MU-GSSK-SCD with Perfect CSI

In the first scenario presented in Fig. 2a, the legitimate users are located at opposing corners of the room, precisely at $[-2, 2, 0.85]$ and $[2, -2, 0.85]$. For this scenario, the eavesdropper is located in three different locations: a) closer to User 1, b) in the middle of the users, c) closer to User 2. The corresponding BER curves are obtained and presented in Fig. 3, in the given order. In all BER graphs, four curves are generated: two of them represent the BERs of User 1 and User 2. Eve's performance is exhibited in two distinct cases, where it wiretaps User 1 and User 2 respectively, hence two BER curves are obtained for Eve. The simulation results indicate that the eavesdropper suffers from high BERs, which are around the 0.5 level, regardless of the user Eve is wiretapping. Another observation is that the impact of Eve's location on its BER is not significant.

The BER performances under Scenario 2 and Scenario 3 are presented in Figs. 4 and 5 respectively. In Scenario 2, the legitimate users are placed parallel to the $x-$axis, whereas in Scenario 3, they are deliberately chosen very close to each other. The simulation results show that, for all featured user configurations, the BER performance of the MU-GSSK-SCD is almost identical. The results suggest that the proposed solution provides significantly lower BERs to legitimate users than to the eavesdropper regardless of legitimate users' and Eve's locations. Meanwhile, Eve's BER performance is greatly reduced by our design.

B. Practical System Design Considerations

To demonstrate insight into the system design, in the following, we vary several parameters such as the number of transmitting and receiving antennas, the user, and eavesdropper configurations within the indoor environment to investigate how secrecy capacity, as well as BER, affect the system design. First, in Fig. 6, we present the secrecy rate regions obtained by MU-GSSK-SCD with varying number of PDs ($N_r \in \{1, 2, 4\}$) at the users and Eve. In this case, $N_t = 16$ and $N_a = 8$ are assumed, and 6 bits are transmitted to each

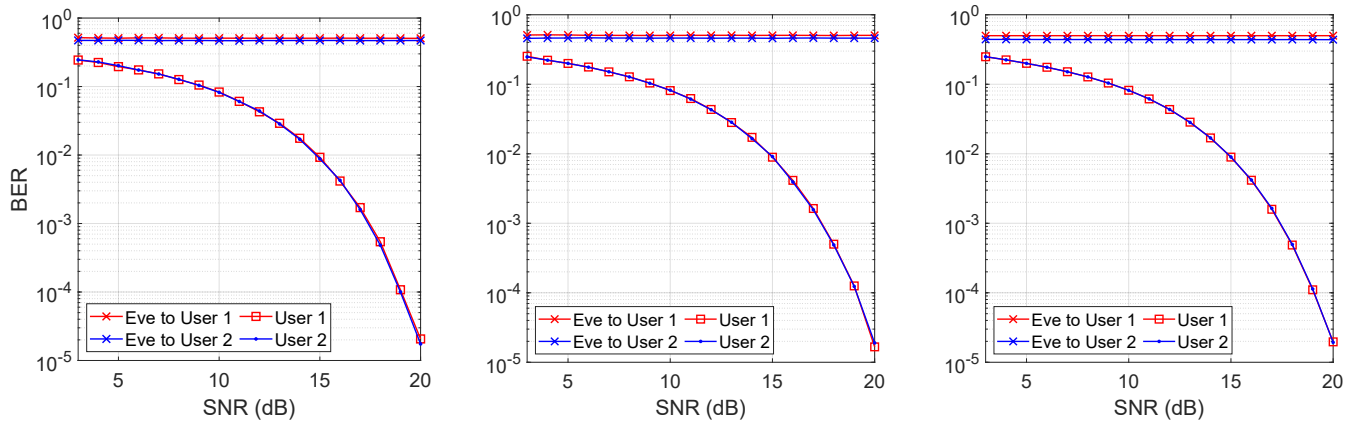

(a) (b) (c)

Fig. 3: BERs for Scenario 1. Eve is located at a) [-1, 1, 0.85], b) [0, 0, 0.85], c) [1, -1, 0.85].

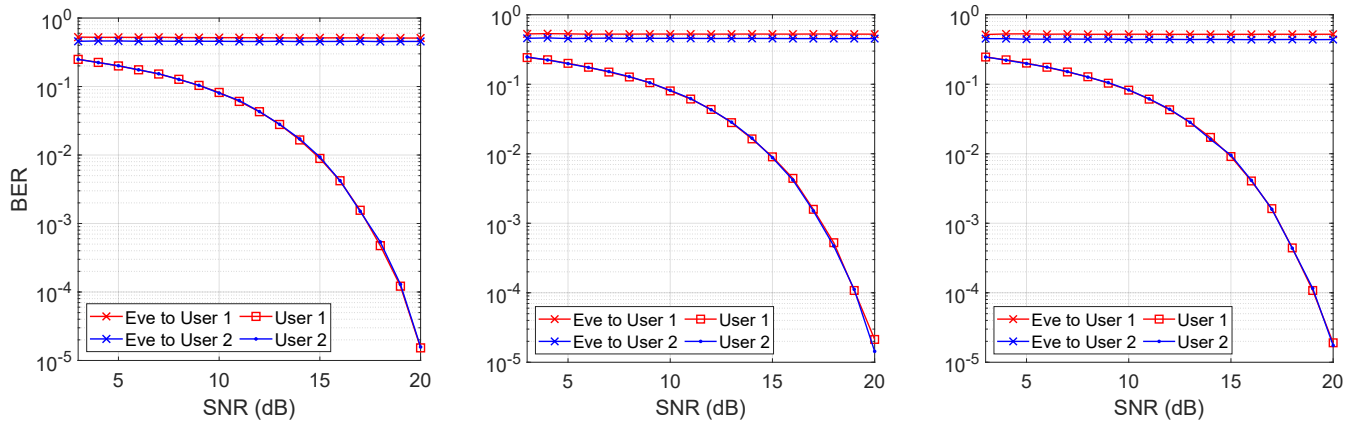

(a) (b) (c)

Fig. 4: BERs for Scenario 2. Eve is located at a) [-1.5, -0.375, 0.85], b) [-0.5, -0.25, 0.85], c) [0.5, -0.125, 0.85].

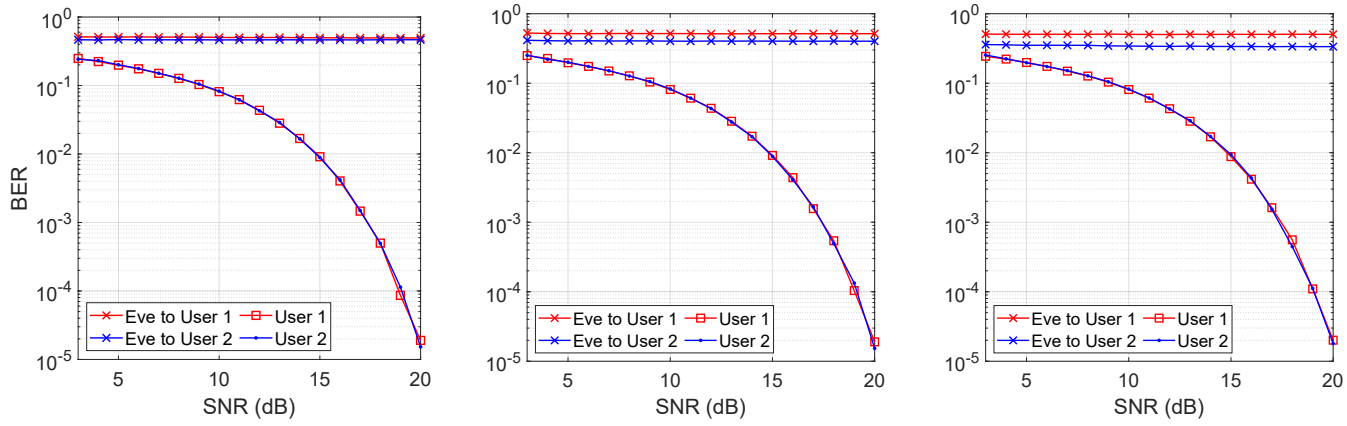

(a) (b) (c)

Fig. 5: BERs for Scenario 3. Eve is located at a) [1.125, -1, 0.85], b) [1.25, -1, 0.85], c) [1.375, -1, 0.85].

user at every signaling interval. It is observed that when the users are equipped with a single PD, the maximum secrecy rate barely exceeds 3 bpcu per user, even at 27 dB SNR, which is considered to be a high SNR value. By installing an extra PD to each user ($N_r = 2$), it is possible to increase the maximum secrecy rate very close to the upper bound, which is 6 bpcu, even at low SNR values, such as 0 dB. Furthermore, it is shown that when the users communicate with 4 PDs, the secrecy rate region reaches the 6 bpcu upper bound at 0 dB SNR. These results indicate that the number of PDs at the receiver circuits play a significant role in terms of PLS. Secondly, we investigate the effect and dependence

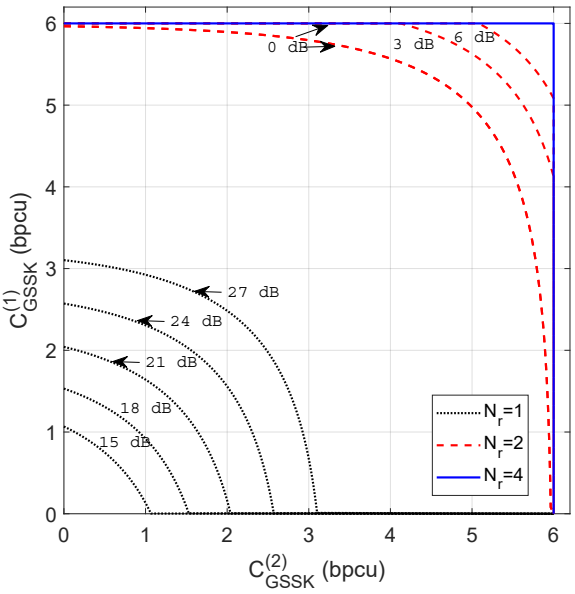

Fig. 6: Secrecy rate regions obtained by MU-GSSK-SCD with $N_t = 16$, $N_a = 8$ and varying N_r.

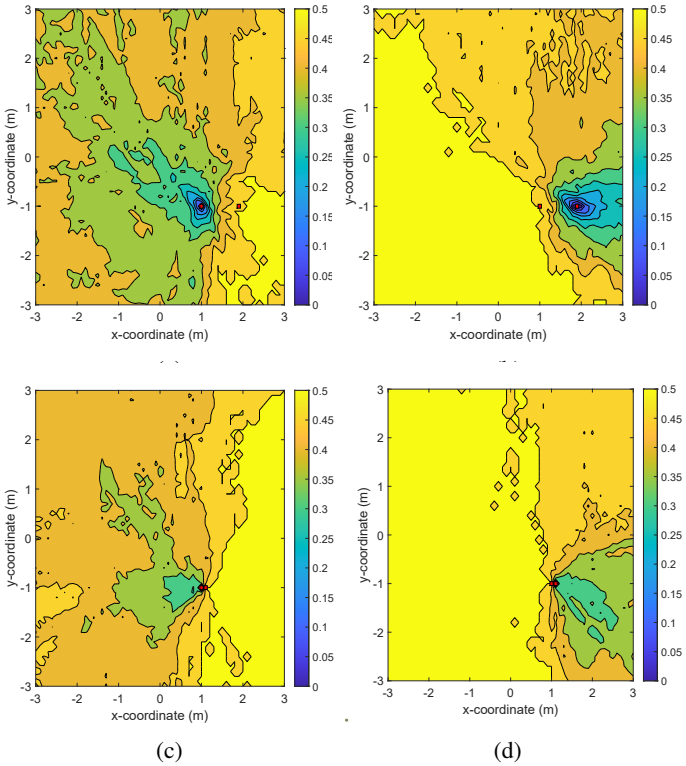

(c) (d)

Fig. 7: BER performance of Eve as it moves within the indoor environment; (a) and (c) when Eve listens to User 1, (b) and (d) when Eve listens to User 2. The User 1 is located at $[1, \ -1]$, where User 2 is located at $[1.9, \ -1]$ and $[1.1, \ -1]$ in (a)-(b) and (c)-(d), respectively. All the units are in meters.

of different user's configuration as well as Eve's location on the BER performance obtained by Eve. To illustrate this, the simulation results in Fig. 7 are obtained, where the BER of Eve is measured by Monte Carlo simulations as it moves within the indoor environment. Figs. 7(a) and 7(b) represent the BER performance of Eve, listening to User 1 and User 2 respectively. Note that, in these figures, both users are denoted by red squares, and located relatively far from each other. The BER level of Eve is denoted by color, and the BER-to-color mapping is shown next to the plots. It is observed that Eve's BER is greater than or equal to 0.3 on almost every point in the environment, however, it improves to the 0.1 level as Eve gets closer to the user she is listening to. When the users are located close to each other, refer to Figs. 7(c) and 7(d), it is observed that the BER performance of Eve is around 0.5 levels in a very wide region of the environment. Additionally, in this case, Eve obtains reduced BERs in a much smaller region, compared to the former case. These results indicate that the proposed MU-GSSK-SCD strategy ensures poor BER performance for Eve almost everywhere, especially when the users are closely located to each other.

C. BER Performance of MU-GSSK-SCD with Imperfect CSI

In the previous subsection, it is shown that MU-GSSK-SCD provides very good BER performance for the GSSK based VLC system when perfect CSI is available at all terminals. However, since the CSI may not always be fully known in real applications, it is very important to analyze the sensitivity of the proposed security solution to channel estimation errors. Following (13) with the optimum LED power vector in (20), the received signals by the legitimate users can be expressed as:

$$\mathbf{y}_k = \rho \mathbf{G} \mathbf{v}_{k,i_k} + \mathbf{n}_k, \quad k = 1, 2, \ldots, K, \tag{41}$$

where $\mathbf{G} \in \mathcal{R}^{KN_r \times KN_r}$ is defined as $\mathbf{G} = \tilde{\mathbf{H}} \left(\tilde{\mathbf{H}}^T \tilde{\mathbf{H}} \right)^{-1} \tilde{\mathbf{H}}^T$. As explained in Section III-A, the parameter ρ is related with the channel coefficients in a nonlinear fashion and requires the knowledge of CSI perfectly both at the receivers and the transmitter. Also, under the perfect CSI at the transmitter, it is shown in Section III that $\mathbf{G}$ is a unit diagonal matrix. We now show that even if the CSI is not perfectly known at receiver, the optimal data detection is not affected by this imperfection.

Assume that the channel coefficient matrix $\mathbf{H}$ is known at the receiver with an error $\mathbf{E}$. Then, the estimated channel matrix $\widehat{\mathbf{H}}$ can be expressed in terms of the error-free channel matrix $\mathbf{H}$ as

$$\mathbf{H} = \widehat{\mathbf{H}} + \mathbf{E}.$$

Substituting this into the expression of $\mathbf{G}$ above, we have

$$\begin{aligned} \widehat{\mathbf{G}} &= (\widehat{\mathbf{H}} + \mathbf{E}) \left((\widehat{\mathbf{H}} + \mathbf{E})^T (\widehat{\mathbf{H}} + \mathbf{E}) \right)^{-1} (\widehat{\mathbf{H}} + \mathbf{E})^T \\ &= \mathbf{I}_{2N_r}. \end{aligned} \tag{42}$$

Consequently, the transmitted signal $\mathbf{v}_{\mathbf{k},\mathbf{i_k}}$ can be recovered optimally by the ML detection using the received signal $\mathbf{y}_k = \rho \mathbf{v}_{k,i} + \mathbf{n}_k$. However, true value of ρ is not known at the k^{th} user, hence needs to be estimated as accurate as possible from the received signal $\mathbf{y}_k$, by means of some pilot GSSK symbols prior to data detection at receiver. In the following, we explain the estimation of ρ based on the ML criterion.

1) ML Estimation of ρ: The power normalization coefficient ρ can be estimated at the k^{th} user by transmitting pilot symbols $\mathbf{s}_p = [\mathbf{s}_{p,1}^T, \mathbf{s}_{p,2}^T, \ldots, \mathbf{s}_{p,K}^T]^T$, which are chosen from the joint symbol alphabet $\mathcal{C}_S$. For independent and identically distributed pilot symbols, the likelihood function for ρ is defined as

$$\hat{\ell}(\rho; \mathbf{y}_k) = \frac{1}{N_p} \sum_{\ell=1}^{N_p} \ln f(\mathbf{y}_{k,\ell}|\rho), \tag{43}$$

where $\mathbf{y}_{k,\ell}$ is the ℓ^{th} received pilot symbol at the k^{th} user. The conditional probability density function (pdf) of $\mathbf{y}_k$ given ρ, $f(\mathbf{y_{k,\ell}}|\rho)$, is found for the ℓ^{th} pilot symbol $\mathbf{s}_{p,\ell}$ using the observation equation in (19) as follows.

$$\ln f(\mathbf{y}_{k,\ell}|\rho) = \ln\left(\frac{(2\pi)^{N_r/2}}{|\mathbb{C}_{\mathbf{n}_k}|^{1/2}}\right) - \frac{||\mathbf{y}_{k,\ell} - \rho\mathbf{s}_p||^2}{2},$$

for $\ell = 1, 2, \cdots, N_p$. Maximizing (43) with respect to ρ, the ML estimate of ρ is found as

$$\widehat{\rho} = \arg\max_{\rho}\{\hat{\ell}(\rho; \mathbf{y}_k)\} = \frac{1}{N_p} \sum_{\ell=1}^{N_p} \frac{\mathbf{y}_{k,\ell}^T \mathbf{s}_{p,\ell}}{\mathbf{s}_{p,\ell}^T \mathbf{s}_{p,\ell}}. \tag{44}$$

The estimation accuracy can be measured in terms of the root mean square of the error $\rho - \hat{\rho}$, which is defined by

$$\text{RMSE}(\hat{\rho}) = \frac{1}{N_p} \sum_{\ell=1}^{N_p} ||\rho - \hat{\rho}||^2. \tag{45}$$

Next, the MU-GSSK-SCD system is simulated with imperfect CSI, when there are 2 users, located according to the Scenario 1 from Fig. 2. For each SNR point, $N_p = 1000$ pilot symbols are broadcasted to users, which then estimate the power normalization coefficient as found in (44). The obtained RMSE values for $\hat{\rho}$ are normalized and presented in Fig. 8. It is observed that the ML estimation resulted in an RMSE of 0.95ρ for 3 dB SNR. The RMSE is reduced exponentially down to 0.12ρ at 20 dB SNR. The BER performance of the proposed system with the estimated ρ values is presented in Fig. 9. In this figure, the dashed curves represent the case where the users have full CSI, therefore ρ can be perfectly calculated at the users and RMSE becomes zero. It is observed that due to the estimation errors at the users, there is a loss of 2 to 3 dB SNR. However, the BER is obtained around 10^{-3} level at the high SNR band, which is an acceptable range for indoor VLC applications. Thus, the proposed MU-GSSK-SCD system provides excellent BER performance with negligible sensitivity to receiver CSI.

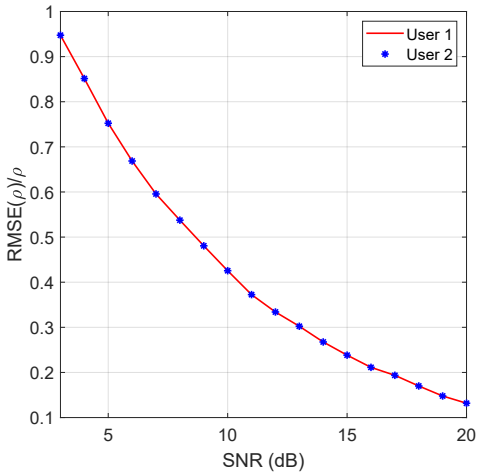

Fig. 8: Root mean square of the estimation error $||\rho - \hat{\rho}||$ for Scenario 1, under the imperfect CSI at the users.

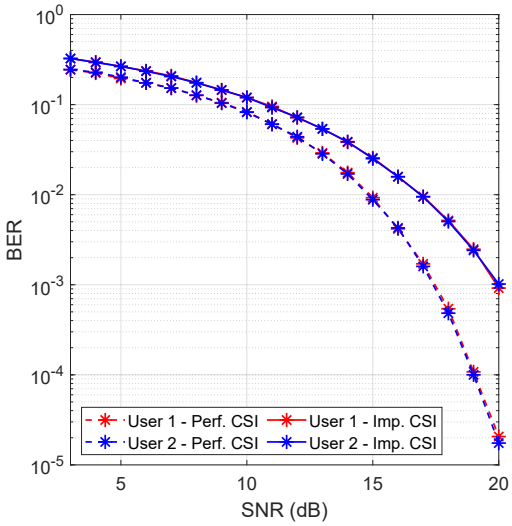

Fig. 9: BER vs. SNR plots for Scenario 1 under the imperfect CSI at the users.

D. Comparison of Results with Existing Ones

Regarding comparing the results with existing ones, we considered the most appropriate ones in the existing literature, which are based on PLS techniques aided by friendly jamming with a DC-biased 8-level pulse amplitude modulation (8-PAM) scheme transmitted via single LED. At the receiver, the DC-bias is removed and data is recovered by the classical ML detection. The jammer was equipped with multiple LEDs without access to the transmitted information. Assuming that accurate CSI of the eavesdropper is known by the source, an optimal jamming beamformer was designed that degrades the eavesdropper's reception of the secured information sent to the legitimate users. We set the transmit powers of each system to unity for a fair comparison. For the 8-PAM-PLS system based on generating a friendly jamming signal, we reduced the average power of the transmitted data in the amount of the power of the jamming signal to keep equal transmitted power for both PLS systems. In Figure 10, we compare the BER performance of this technique, with the PLS-GSSK system having the same system parameters. Specifically, both VLC systems have $N_t = 8$ LEDs at the transmitter side designed with 3 bits/sec/Hz spectral efficiency each. We set the transmit powers of each system to unity for a fair comparison. Each BER curve of the PAM-PLS system in Figure 10 corresponds to the case where a certain percentage of the total transmit power is used for generating jamming signal, which is transmitted towards the eavesdropper. As can be seen from these curves, the BER performance of the

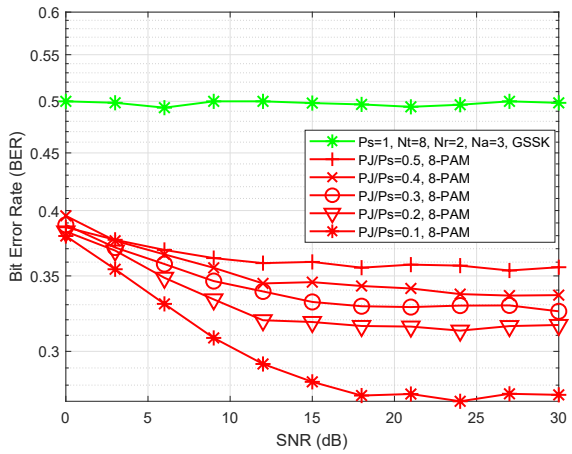

Fig. 10: Eve's BER vs. SNR curves for 8-PAM and GSSK with 3 bits/sec/Hz per user.

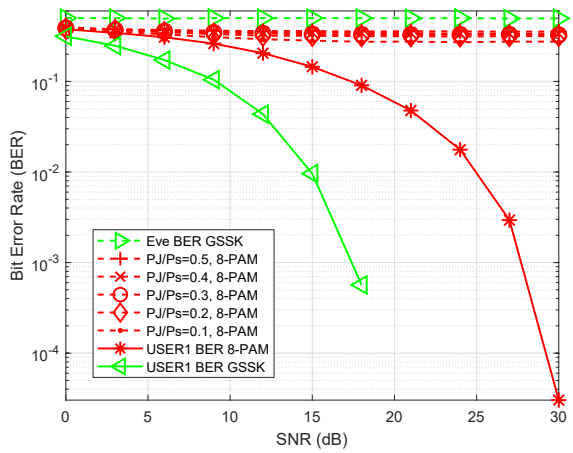

Fig. 11: Bob's and Eve's BER vs. SNR curves for 8-PAM and GSSK with 3 bits/sec/Hz per user.

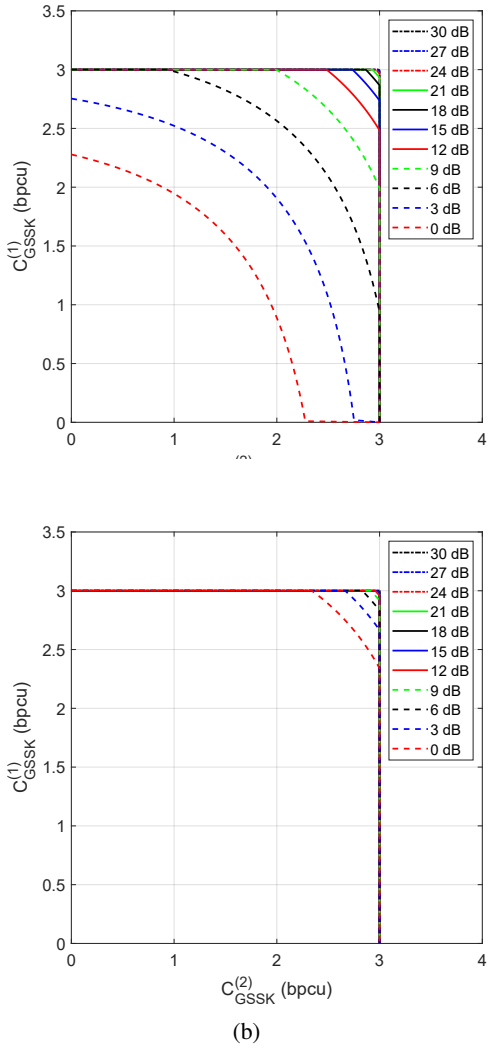

Fig. 12: Secrecy rate regions when the users are, a) 30 cm and b) 90 cm apart.

PAM-PLS system is uniformly worse than that of the PLS-GSSK system. Figure 11 compares the BER performances of the legitimate users employing one of the PLS techniques mentioned above. The figure shows clear superiority of the proposed PLS scheme, since, for example, the obtained gain in SNR is more than 15 dB at a BER of 10^{-3}. In addition to the degraded BER performances of the PAM-PLS systems, the assumption that the eavesdropper's CSI should be accurately known to the source is not a realistic one and hence, the performance curves provided in Figure 10 can only be an upper bound in the real applications.

E. Secrecy Performance

In this subsection, the secrecy rate regions defined in (37) and (38) are found for the proposed MU-GSSK-SCD strategy. First, both users are placed 30 cm apart at $[1, -1, 0.85]$ and $[1.3, -1, 0.85]$ and Eve is located in the middle of the two. The secrecy rate regions for this specific configuration is presented in Fig. 12(a). It is observed that, around $0 - 3$ dB SNR, the secrecy rates of the users are around $2 - 2.5$ bpcu and increase approximately with 0.16 bpcu/dB in SNR. At around 6 dB SNR, the secrecy rate of both users get very close to 3 bpcu, which is the maximum for 8-QAM communication. In another configuration, the users are located at $[1, -1, 0.85]$ and $[1.9, -1, 0.85]$ and Eve is located closer to one of the users at $[1.15, -1, 0.85]$. The secrecy rate regions for this configuration are presented in Fig. 12(b), which indicates that even at 0 dB SNR level, users can communicate with almost full secrecy. These results show that the PLS obtained with MU-GSSK-SCD improves as the users move away from each other. In Fig. 13, the secrecy performance of MU-GSSK-SCD is presented for 0 dB SNR in the same user configuration from Fig. 12(b), while Eve is moving straight away from User 1 to User 2. In this setting, the minimal separation of Eve to any user is $\min\{x, 90 - x\}$ cm, where x is the distance of Eve to User 1 as indicated in the legend. Note that, similar rate regions are obtained at identical minimal separations. It is observed that the achievable secrecy rate region enlarges as the minimal separation of Eve to any user increases. In fact,

when the distance of Eve to any user is larger than 25 cm, the achievable secrecy rate region reaches its maximum size. These results indicate that PLS provided by MU-GSSK-SCD depends on Eve's location for a fixed user configuration. Also, MU-GSSK-SCD can provide maximal secrecy rates with 2 users positioned at a 90 cm separation from each other, hence PLS is

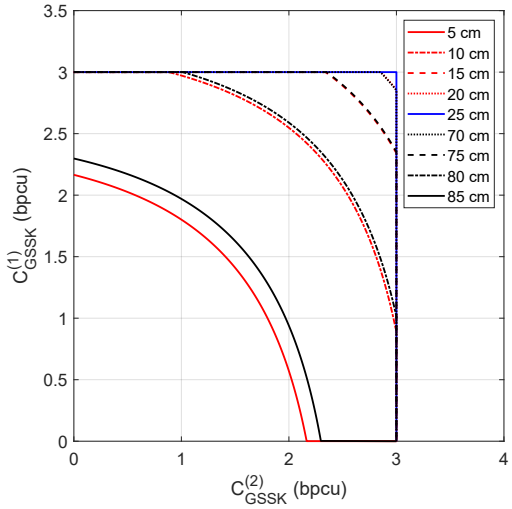

Fig. 13: Secrecy rate regions for SNR of 0 dB while Eve moving away from User 1 to User 2. The separation values between the User 1 and Eve are indicated in the legend.

F. Computational Complexity Analysis

Computational issue arises in the proposed multi user PLS system, during precoding at the transmitter and data detection at the receiver. The source transmits data to the users via suitably designed linear regularized zero-forcing precoder, that can be computed according to (24) as

$$\mathbf{P}_k = \rho \tilde{\mathbf{H}}_k \left(\tilde{\mathbf{H}}^T \tilde{\mathbf{H}} + \epsilon \mathbf{I}_{N_a} \right)^{-1} \tilde{\mathbf{H}}^T \mathbf{v}_{\mathcal{S},s}, \tag{46}$$

where, $\tilde{\mathbf{H}} \in R^{N_r \times N_a}$ denotes the channel matrix between the source and the kth user, ρ is the power normalization factor and ϵ is the regularization parameter. In the above, matrix multiplication needs roughly $\mathcal{O}(N_r N_a^2)$ operations, and matrix inversion requires approximately $\mathcal{O}(N_a^3)$ operations. On the other end, when the transmitter precoding is capable of perfectly separating K users, low-complexity single stream detection is facilitated at the receiver. According to the received signal at the kth user

$$\mathbf{y}_k = \mathbf{s}_k + \mathbf{n}_k, \quad k = 1, 2, \cdots, K, \tag{47}$$

where $\mathbf{s}_k$ is the observed transmitted signal by the k^{th} user and given by (24), the detection complexity increases linearly with K. Hence, the total complexity of the detection of signals at users is $\mathcal{O}(K M_k N_a)$ where M_k is the constellation size of the kth user's received signal. Hence, in summary, the MU-GSSK based PLS scheme proposed in this paper has approximately complexity of $\mathcal{O}(N_r N_a^2 + N_a^3 + K M_k N_a)$.

VI. Conclusion

In this paper, we have presented a PLS technique to enhance the security of multiuser VLC systems in the presence of an eavesdropper. A novel design of spatial constellations has been proposed for the MIMO-GSSK based scheme to maximize the minimum Euclidean distance of the transmit symbol set with the aid of CSI of the legitimate users. A zero-forcing precoder was also constructed at the transmitter by optimally reshaping the GSSK signal with the legitimate users' CSI to minimize their BERs. The signal shaping with precoding approach also acts as that of a friendly jammer that degrades the Eve's communication and SNR severely so as to prevent any meaningful confidential message leakage to Eve. In addition, the legitimate users' secrecy region was derived and shown by computer simulations that the proposed PLS technique effectively sends secure information to the multiple legitimate users and prohibits the reception of the same information by eavesdropper successfully in terms of the BER performance. It was also shown that the BER performances of the legitimate users were not very sensitive to parameter estimation errors under imperfect receiver CSI. Furthermore, it has been observed that for the same SNR level, the secrecy region was enlarged as the legitimate user separation increases, and full secrecy could be achieved at 0 dB SNR, when the user separation was 90 cm.

References

[1] J. G. Andrews, S. Buzzi, W. Choi, S. V. Hanly, A. Lozano, A. C. K. Soong, and J. C. Zhang, "What will 5G be?" *IEEE J. Sel. Areas Commun.*, 2014.

[2] I. Stefan, H. Burchardt, and H. Haas, "Area spectral efficiency performance comparison between VLC and RF femtocell networks," in *Proc. IEEE ICC*, 2013, pp. 3825–3829.

[3] A. Mostafa and L. Lampe, "Physical-layer security for indoor visible light communications," in *Proc. IEEE ICC)*, 2014, pp. 3342–3347.

[4] I. E. Telatar, "Capacity of multi-antenna gaussian channels," *Tech. Rep. Bell Labs, Lucent Technologies*, pp. ,, 1995.

[5] F. Oggier and B. Hassibi, "The secrecy capacity of the MIMO wiretap channel," *IEEE Trans. Inf. Theory*, vol. 57, no. 8, pp. 4961–4972, 2011.

[6] Y. Wu, A. Khisti, C. Xiao, G. Caire, K. Wong, and X. Gao, "A survey of physical layer security techniques for 5G wireless networks and challenges ahead," *IEEE J. Sel. Areas Commun*, 2018.

[7] A. Mostafa and L. Lampe, "Securing visible light communications via friendly jamming," in *Proc. 2014 IEEE GC Wkshps*, 2014, pp. 524–529.

[8] M. A. Arfaoui, Z. Rezki, A. Ghrayeb, and M. S. Alouini, "On the secrecy capacity of MISO visible light communication channels," in *Proc. IEEE GLOBECOM*, 2016, pp. 1–7.

[9] S. Ma, Z. Dong, H. Li, Z. Lu, and S. Li, "Optimal and robust secure beamformer for indoor MISO visible light communication," *J. Lightw. Technol.*, vol. 34, no. 21, pp. 4988–4998, 2016.

[10] A. Mukherjee, "Secret-key agreement for security in multi-emitter visible light communication systems," *IEEE Commun. Lett.*, vol. 20, no. 7, pp. 1361–1364, 2016.

[11] O. Hassan, E. Panayirci, H. V. Poor, and H. Haas, "Physical-layer security for indoor visible light communications with space shift keying modulation," in *Proc. IEEE GLOBECOM*, 2018, pp. 1–6.

[12] M. A. Arfaoui, H. Zaid, Z. Rezki, A. Ghrayeb, A. Chaaban, and M. Alouini, "Artificial noise-based beamforming for the MISO VLC wiretap channel," *IEEE Trans. Commun.*, vol. 67, no. 4, pp. 2866–2879, 2019.

[13] M. A. Arfaoui, A. Ghrayeb, and C. M. Assi, "Secrecy performance of the MIMO VLC wiretap channel with randomly located eavesdropper," *IEEE Trans. Wireless Commun.*, vol. 19, no. 1, pp. 265–278, 2020.

[14] M. A. Arfaoui, M. D. Soltani, I. Tavakkolnia, A. Ghrayeb, M. Safari, C. M. Assi, and H. Haas, "Physical layer security for visible light communication systems: A survey," *IEEE Commun. Surveys Tuts.*, vol. 22, no. 3, pp. 1887–1908, 2020.

[15] E. Panayirci, A. Yesilkaya, T. Cogalan, H. V. Poor, and H. Haas, "Physical-layer security with optical generalized space shift keying," *IEEE Trans. Commun.*, vol. 68, no. 5, pp. 3042–3056, 2020.

[16] A. Yesilkaya, T. Cogalan, S. Erkucuk, Y. Sadi, E. Panayirci, H. Haas, and H. V. Poor, "Physical-layer security in visible light communications," in *2nd 6G Wireless Summit (6G SUMMIT)*, 2020, pp. 1–5.

[17] A. Mukherjee, S. A. A. Fakoorian, J. Huang, and A. L. Swindlehurst, "Principles of physical layer security in multiuser wireless networks: A survey," *IEEE Commun. Surveys Tuts.*, vol. 16, no. 3, pp. 1550–1573, 2014.

[18] L. Fan, N. Yang, T. Q. Duong, M. Elkashlan, and G. K. Karagiannidis, "Exploiting direct links for physical layer security in multiuser multirelay networks," *IEEE Trans. Wireless Commun.*, vol. 15, no. 6, pp. 3856–3867, 2016.

[19] F. Shu, X. Wu, J. Hu, J. Li, R. Chen, and J. Wang, "Secure and precise wireless transmission for random-subcarrier-selection-based directional modulation transmit antenna array," *IEEE J. Sel. Areas Commun.*, vol. 36, no. 4, pp. 890–904, 2018.

[20] T. V. Pham, T. Hayashi, and A. T. Pham, "Artificial-noise-aided precoding design for multi-user visible light communication channels," *IEEE Access*, vol. 7, pp. 3767–3777, 2019.

[21] T. Shen, S. Zhang, R. Chen, J. Wang, J. Hu, F. Shu, and J. Wang, "Two practical random-subcarrier-selection methods for secure precise wireless transmissions," *IEEE Trans. Veh. Technol.*, vol. 68, no. 9, pp. 9018–9028, 2019.

[22] J. Choi, J. Joung, and B. C. Jung, "Space–time line code for enhancing physical layer security of multiuser MIMO uplink transmission," *IEEE Syst. J.*, pp. 1–12, 2020.

[23] R. Y. Mesleh, H. Haas, S. Sinanovic, C. W. Ahn, and S. Yun, "Spatial modulation," *IEEE Trans. Veh. Technol.*, vol. 57, no. 4, pp. 2228–2241, 2008.

[24] R. Mesleh, H. Elgala, and H. Haas, "Optical spatial modulation," *IEEE J. Opt. Commun. Netw.*, vol. 3, no. 3, pp. 234–244, 2011.

[25] Y. A. Chau and Shi-Hong Yu, "Space modulation on wireless fading channels," in *Proc. IEEE 54th VTC Fall 2001, Cat. No.01CH37211*, vol. 3, 2001, pp. 1668–1671 vol.3.

[26] H. Haas, E. Costa, and E. Schulz, "Increasing spectral efficiency by data multiplexing using antenna arrays," in *Proc. IEEE PIMRC*, vol. 2, 2002, pp. 610–613 vol.2.

[27] J. Jeganathan, A. Ghrayeb, and L. Szczecinski, "Generalized space shift keying modulation for MIMO channels," in *Proc. IEEE PIMRC*, 2008, pp. 1–5.

[28] W. Popoola, E. Poves, and H. Haas, "Generalised space shift keying for visible light communications," in *Proc. 8th Int. symp. CSNDSP*, 2012, pp. 1–4.

[29] W. O. Popoola, E. Poves, and H. Haas, "Error performance of generalised space shift keying for indoor visible light communications," *IEEE Trans. Commun.*, vol. 61, no. 5, pp. 1968–1976, 2013.

[30] L. Yang, "Transmitter preprocessing aided spatial modulation for multiple-input multiple-output systems," in *Proc. IEEE VTC Spring*, 2011, pp. 1–5.

[31] S. Sinanovic, N. Serafimovski, M. Di Renzo, and H. Haas, "Secrecy capacity of space keying with two antennas," in *IEEE VTC Fall*, 2012, pp. 1–5.

[32] S. R. Aghdam and T. M. Duman, "Secure space shift keying transmission using dynamic antenna index assignment," in *Proc. IEEE GLOBECOM*, 2017, pp. 1–6.

[33] F. Wang, C. Liu, Q. Wang, J. Zhang, R. Zhang, L. Yang, and L. Hanzo, "Secrecy analysis of generalized space-shift keying aided visible light communication," *IEEE Access*, vol. 6, pp. 18 310–18 324, 2018.

[34] ——, "Optical jamming enhances the secrecy performance of the generalized space-shift-keying-aided visible-light downlink," *IEEE Trans. Commun.*, vol. 66, no. 9, pp. 4087–4102, 2018.

[35] Y. Chen, L. Wang, Z. Zhao, M. Ma, and B. Jiao, "Secure multiuser MIMO downlink transmission via precoding-aided spatial modulation," *IEEE Commun. Lett.*, vol. 20, no. 6, pp. 1116–1119, 2016.

[36] T. V. Pham and A. T. Pham, "On the secrecy sum-rate of MU-VLC broadcast systems with confidential messages," in *Proc. 10th Int. Symp. on Communication Systems, Networks and Digital Signal Processing (CSNDSP)*, 2016, pp. 1–6.

[37] C. Chen, D. A. Basnayaka, and H. Haas, "Downlink performance of optical attocell networks," *J. Lightw. Technol.*, vol. 34, no. 1, pp. 137–156, 2016.

[38] A. Al-Kinani, C. Wang, L. Zhou, and W. Zhang, "Optical wireless communication channel measurements and models," *IEEE Commun. Surv. Tutor.*, vol. 20, no. 3, pp. 1939–1962, 2018.

[39] J. M. Kahn and J. R. Barry, "Wireless infrared communications," *Proc. IEEE*, vol. 85, no. 2, pp. 265–298, 1997.

[40] H. Burchardt, N. Serafimovski, D. Tsonev, S. Videv, and H. Haas, "VLC: Beyond point-to-point communication," *IEEE Commun. Mag.*, vol. 52, no. 7, pp. 98–105, 2014.

[41] J. Shi, J. He, K. Wu, and J. Ma, "Enhanced performance of asynchronous multi-cell VLC system using OQAM/OFDM-NOMA," *J. Lightw. Technol.*, vol. 37, no. 20, pp. 5212–5220, Oct 2019.

[42] H. Yang, C. Chen, and W. Zhong, "Cognitive multi-cell visible light communication with hybrid underlay/overlay resource allocation," *IEEE Photon. Technol. Lett.*, vol. 30, no. 12, pp. 1135–1138, June 2018.

[43] C. Tran, T. Hoang, and N. Nguyen, "Coordinated multi-channel transmission scheme for indoor multiple access points VLC networks," in *19th ISCIT*, Sep. 2019, pp. 611–615.

[44] A. Yesilkaya, T. Cogalan, E. Panayirci, H. Haas, and H. V. Poor, "Achieving minimum error in MISO optical spatial modulation," in *Proc. IEEE ICC*, 2018, pp. 1–6.

[45] A. A. Purwita, A. Yesilkaya, I. Tavakkolnia, M. Safari, and H. Haas, "Effects of irregular photodiode configurations for indoor MIMO VLC with mobile users," in *Proc. IEEE PIMRC*, 2019, pp. 1–7.

[46] A. M. Khalid, G. Cossu, R. Corsini, P. Choudhury, and E. Ciaramella, "1-Gb/s transmission over a phosphorescent white LED by using rate-adaptive discrete multitone modulation," *IEEE Photon. J.*, vol. 4, no. 5, pp. 1465–1473, 2012.

[47] A. Tsiatmas, C. P. M. J. Baggen, F. M. J. Willems, J. M. G. Linnartz, and J. W. M. Bergmans, "An illumination perspective on visible light communications," *IEEE Commun. Mag.*, vol. 52, no. 7, pp. 64–71, 2014.

[48] S. Leung-Yan-Cheong and M. Hellman, "The Gaussian wire-tap channel," *IEEE Trans. Inf. Theory*, vol. 24, no. 4, pp. 451–456, 1978.

[49] T. M. Cover and J. A. Thomas, *Elements of Information Theory (Wiley Series in Telecommunications and Signal Processing)*. USA: Wiley-Interscience, 2006.

[50] R. S. Cheng, "Multirate achievability in memoryless multiaccess channel," in *Proc. IEEE ISIT*, 1994, pp. 58–.

Nuğman Su (Student Member, IEEE) received the B.Sc. and M.Sc. degrees in electrical and electronics engineering from Boğaziçi University, Istanbul, Turkey, in 2012 and 2015, respectively. He is currently pursuing the Ph.D. degree in electrical and electronics engineering with Boğaziçi University. His research interests are on physical layer security and optimum communication strategies, particularly in optical communications.

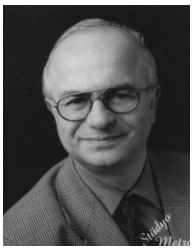

Erdal Panayirci (M'80-SM'91-F'03-LF'06) received the Diploma Engineering degree in electrical engineering from Istanbul Technical University, Istanbul, Turkey, in 1964, and the Ph.D. degree in electrical engineering and system science from Michigan State University, MI, USA, in 1971. He is currently a Professor at the Electrical and Electronics Engineering Department, Kadir Has University, Istanbul, Turkey and Visiting Research Collaborator at the Department of Electrical Engineering, Princeton University, NJ, USA. He spent the academic years 2008–2009 and 2017–2018 with the Department of Electrical Engineering, Princeton University. He has published extensively in leading scientific journals and international conference and co-authored the book Principles of Integrated Maritime Surveillance Systems (Kluwer Academic, 2000). His research interests include communication theory, synchronization, advanced signal processing techniques and their applications to wireless electrical, underwater and optical communications.

Dr. Panayirci was an Editor for the IEEE TRANSACTIONS ON COMMUNICATIONS in the areas of Synchronization and Equalization during 1995–2000. He served and is currently serving as a Member of IEEE Fellow Committee during 2005–2008 and 2018– 2020, respectively. He is currently a member of the IEEE GLOBECOM/ICC Management and Strategy Standing Committee. He was the Technical Program Co-Chair of the IEEE International Conference on Communications (ICC2006) and the Technical Program Chair of the IEEE PIMRC, both held in Istanbul in 2006 and 2010, respectively. He was the Executive Vice Chairman of the IEEE Wireless Communications and Networking Conference, Istanbul, Turkey, in April 2014. He was the General Co-Chair of the IEEE PIMRC held in Istanbul, Turkey, in September 2019.

Mutlu Koca (S'99-M'02-SM'17) Mutlu Koca received his B.Sc. degrees in Electrical Engineering and Physics from Boğaziçi University, Istanbul Turkey, in 1996; his M.Sc. degrees in Electrical Engineering and Applied Mathematics in 2000 and his Ph.D. degree in Electrical Engineering in 2001, all from the University of California at Davis. He has worked as a Senior Design Engineer in Flarion Technologies, Bedminster, NJ, between 2001 and 2003 and as a visiting postdoctoral researcher in Institut de Recherche en Informatique et Systèmes Aléatoires (IRISA), Rennes, France between 2003 and 2004. He joined the Department of Electrical and Electronics Engineering of Boğaziçi University as a faculty member in 2004 where he is currently a full Professor. Between 2010 and 2011, he was also a visiting professor at the Telecommunications Department of CentraleSupélec, Paris, France. Dr. Koca has served on the organization committees of PIMRC 2010 as PHY Area Co-Chair, SPAWC 2012 as TPC Co-Chair, WCNC 2014, BlackSeaCom 2015 and PIMRC 2019 as Publications Chair. He is serving as the Publications Chair of WCNC 2020 and Globecom 2021. His research interests are on wireless communications, optical communications, information theory and signal processing.

Anil Yesilkaya (S'11) received the B.Sc. (Hons.) and M.Sc. degrees in electronics engineering from Kadir Has University, Istanbul, Turkey, in 2014 and 2016, respectively. He is currently pursuing the Ph.D. degree in digital communications with The University of Edinburgh. His research interests include multiple-input multiple-output optical wireless communications and LiFi-based in-flight connectivity. He was a recipient of the Best Paper Award at the IEEE International Conference on Communications (ICC) in 2018.

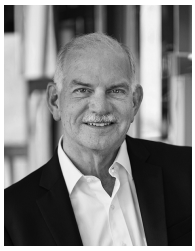

H. Vincent Poor (S'72-M'77-SM'82-F'87) received the Ph.D. degree in EECS from Princeton University in 1977. From 1977 until 1990, he was on the faculty of the University of Illinois at Urbana-Champaign. Since 1990 he has been on the faculty at Princeton, where he is currently the Michael Henry Strater University Professor of Electrical Engineering. During 2006 to 2016, he served as Dean of Princeton's School of Engineering and Applied Science. He has also held visiting appointments at several other universities, including most recently at Berkeley and Cambridge. His research interests are in the areas of information theory, machine learning and network science, and their applications in wireless networks, energy systems and related fields. Among his publications in these areas is the recent book Multiple Access Techniques for 5G Wireless Networks and Beyond. (Springer, 2019).

Dr. Poor is a member of the National Academy of Engineering and the National Academy of Sciences, and is a foreign member of the Chinese Academy of Sciences, the Royal Society, and other national and international academies. Recent recognition of his work includes the 2017 IEEE Alexander Graham Bell Medal and a D.Eng. honoris causa from the University of Waterloo awarded in 2019.

Harald Haas (S'98-M'03-SM'16-F'17) is the Director of the LiFi Research and Development Centre at the University of Strathclyde. He is also the Initiator, co-founder and Chief Scientific Officer of pureLiFi Ltd. He received the Ph.D. degree from The University of Edinburgh in 2001. He has authored 550 conference and journal papers, including papers in Science and Nature Communications. Haas' main research interests are in optical wireless communications, hybrid optical wireless and RF communications, spatial modulation, and interference coordination in wireless networks. His team invented spatial modulation. He introduced LiFi to the public at an invited TED Global talk in 2011. This talk on Wireless Data from Every Light Bulb has been watched online over 2.72 million times. LiFi was listed among the 50 best inventions in TIME Magazine in 2011. He gave a second TED Global lecture in 2015 on the use of solar cells as LiFi data detectors and energy harvesters. This has been viewed online over 2.75 million times. In 2016, he received the Outstanding Achievement Award from the International Solid State Lighting Alliance. In 2019 he was recipient of IEEE Vehicular Society James Evans Avant Garde Award. Haas was elected a Fellow of the Royal Society of Edinburgh (RSE) in 2017. In the same year he received a Royal Society Wolfson Research Merit Award and was elevated to IEEE Fellow. In 2018 he received a three-year EPSRC Established Career Fellowship extension and was elected Fellow of the IET. Haas was elected Fellow of the Royal Academy of Engineering (FREng) in 2019.